ACS ES&T Water

pubs.acs.org/estwater

Article

Visible Light-Induced Marine Bacterial Inactivation in Seawater by an *In Situ* Photo-Fenton System without Additional Oxidants: Implications for Ballast Water Sterilization

Wanjun Wang, Haojing Xie, Guiying Li, Jia Li, Po Keung Wong, and Taicheng An*

Cite This: *ACS EST Water* 2021, 1, 1483−1494

Read Online

ACCESS | Metrics & More | Article Recommendations | Supporting Information

ABSTRACT: Harmful non-indigenous microorganism invasion caused by ballast water discharge poses severe threats to marine environments. In this study, a conceptual *in situ* photo-Fenton system without additional oxidants was first established for ballast water sterilization. Pyromellitic acid diimine (PDI)-modified g-C_3N_4 was utilized as a photocatalyst to produce H_2O_2, which was *in situ* activated by Fe(II) to produce •OH for deep oxidation. Marine bacterium *Vibrio alginolyticus* (7 log) in ballast seawater was totally inactivated within 35 min of visible light irradiation. Simultaneous bacterial inactivation and H_2O_2 production was monitored to confirm the *in situ* coupling mechanism, and •OH instead of H_2O_2 was determined to be the dominant reactive species. The influence of seawater parameters, such as salinity, pH, and dissolved oxygen, on the inactivation efficiency was revealed. In addition, the bacterial inactivation mechanisms in terms of cell membrane rupture, intracellular enzyme activity, and total protein change were clarified. The organic matter release profile during bacterial lysis was probed by fluorescence excitation−emission matrix technology, which revealed minimal acute toxicity and impacts on the marine environment. This work not only advances an external oxidant-free system for on-board ballast water sterilization using sustainable solar energy but also creates an avenue for exploring bacterial inactivation mechanisms in seawater.

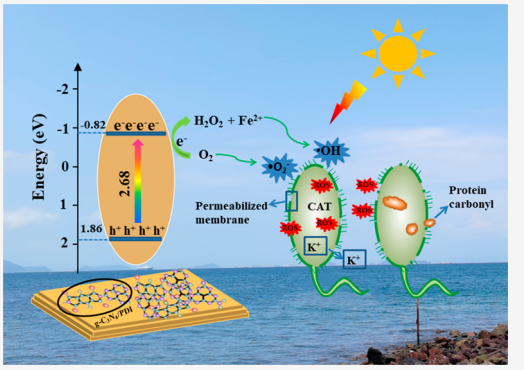

KEYWORDS: *photocatalysis, bacterial inactivation, ballast water, photo-Fenton, marine bacteria*

1. INTRODUCTION

Cargo ships load ballast water to guarantee their stability and operational safety during travel.[1] It has been estimated that 10−30 billion tons of ballast water that contains a wide variety of biota is transferred across the world annually.[2] These non-indigenous aquatic species enter the new natural environment and cause biological invasion, which results in serious ecological damage and economic loss.[3] A notorious example is the discharge of ballast water that led to the invasion of North America by zebra mussel, which cost billions of dollars for the remediation. The potential international dissemination of diseases caused by pathogenic microorganisms from cargo ship ballast water also threatens human health.[4] In response to this issue, the Ballast Water Convention (BWC) was adopted by the United Nations International Maritime Organization (IMO) as an international law in 2004, which requires cargo ships to develop effective ballast water treatment systems to control the invasive species and microorganism contamination. The BWC has been effective since September 2017 and could become more rigorous if amended in future. This convention has stimulated intense research efforts to develop cost-effective technologies for ballast water treatment in recent years.

Current ballast water treatment systems normally include a filtration process to remove large organisms, followed by a sterilization process to control microorganisms such as phytoplankton, bacteria, and viruses. Ballast water sterilization is often realized with ultraviolet (UV) irradiation, chlorination, ozonation, and electrochemical processes.[5−8] However, UV irradiation usually needs to consider the recolonization of bacteria.[9,10] Ozonation has problems of high energy consumption and corrosion of the cabin.[11] Electrochemical methods for producing sodium hypochlorite (NaClO) for sterilization also suffer from high energy input and explosive H_2 gas as byproducts.[12]

In this scenario, an advanced oxidative process (AOPs) based on hydroxyl radical (•OH) formation has been considered as an alternative technology for ballast water sterilization, due to the strong oxidation characteristics of •OH, which has been proven to possess the ability to inactivate various kinds of microorganisms even in high-salinity

Received: February 9, 2021
Revised: April 26, 2021
Accepted: April 27, 2021
Published: May 3, 2021

seawater. For instance, a •OH solution produced by ionization discharge shows high efficacy for ballast water sterilization, which has potential for large-scale on-board application.[13] In addition, the •OH treatment is reported to produce minimal DBPs, which pose no potential risk to the marine environment.[14] However, all of the identified methods require external high energy input, which is not sustainable. Meanwhile, the Fenton system is well-established as one of the most powerful technologies for generating •OH using H_2O_2 as the oxidant in the presence of suitable catalysts. However, the high costs of production, transportation, and storage of H_2O_2 significantly limit its sustainable application.[15]

Fortunately, photocatalytic technology has been recognized as a green and sustainable method for producing H_2O_2 in aquatic environments, because solar energy can be used as the energy source and the photocatalysts can be recycled after use.[16−18] Although the inactivation of pathogenic microorganisms by photocatalysis has been extensively investigated by our group and other groups, most of the attempts were conducted in only pure water or a normal saline system (0.9% NaCl).[19−21] The studies of marine bacterial inactivation in seawater are quite scare. As mentioned above, microorganism inactivation for ballast water/seawater sterilization requires the production of •OH. Therefore, it is hypothesized that the H_2O_2 generated during a photocatalytic process could be coupled with a Fenton system to construct an *in situ* photo-Fenton system for microorganism inactivation in seawater. It should be noted that although traditional photo-Fenton systems using H_2O_2 as the oxidant have been widely investigated,[22] the *in situ* photo-Fenton system without the addition of oxidants has rarely been attempted. Whether the *in situ* photo-Fenton system can be used for microorganism inactivation, especially in a seawater system, remains unclear. In addition, most of the studies of photochemically triggered bacterial inactivation predominantly focused on freshwater bacteria (e.g., *Escherichia coli*), but the feasibility for marine bacteria in seawater has seldom been examined. The underlying bacterial inactivation mechanisms and the influence of inorganic ions in seawater, as well as the toxicity assessment of bacterial cell metabolites and debris after disinfection treatment, on the marine environment have also not been clarified.

In this study, the concept of an oxidant-free *in situ* photo-Fenton system was proposed for application in ballast water sterilization. The key issue for constructing the *in situ* photo-Fenton system was the selection of a highly efficient photocatalyst that can produce H_2O_2 in seawater. Recently, pyromellitic acid diimine (PDI)-modified g-C_3N_4 has been reported to be an environmentally friendly photocatalyst for high-efficiency H_2O_2 production in pure water.[23−25] Therefore, g-C_3N_4/PDI was used as an example photocatalyst to couple with Fe(II) to construct an *in situ* photo-Fenton system. According to the D-2 ballast water discharge standard, the discharge limit of *Vibrio* is 1 colony-forming unit (CFU)/100 mL.[26] In addition, *Vibrio alginolyticus* was the main bacterial species in ballast water, which was commonly used as an indicator organism for ballast water sterilization.[27] Therefore, *V. alginolyticus* was used as a representative ballast water bacterium for inactivation experiments in this study. The feasibility of this system for bacterial inactivation was monitored in light of H_2O_2 production, and with respect to the influence of Fe(II) concentration, pH, and salinity on the inactivation efficiency. In addition, the bacterial inactivation mechanisms, leakage of bacterial cell debris during inactivation, and their potential toxicity risk to the marine environment were systematically investigated. This work is expected to provide not only a novel methodology for on-board ballast water sterilization using abundant sunlight at sea but also an in-depth understanding of the bacterial inactivation mechanisms in seawater.

2. EXPERIMENTAL SECTION

2.1. Materials and Photocatalyst Synthesis. g-C_3N_4/PDI was synthesized using a modified two-step calcination method according to ref 23. Briefly, 15 g of melamine (Aldrich, 99%) was added to a crucible and heated in a muffle furnace for 9 h at 425 °C with a heating rate of 3 °C/min to obtain melem. The produced melem was suspended in distilled water at 100 °C for 8 h to remove residual melamine. Subsequently, the purified melem was uniformly mixed with an equimolar ratio of pyromellitic dianhydride (Aldrich, 99%) in an agate mortar. The mixture was then placed into a crucible with a lid and calcined for 4 h at 325 °C with a heating rate of 7 °C/min. The obtained products of g-C_3N_4/PDI were ground into fine powder before use. The pristine g-C_3N_4 was also made by direct pyrolysis of melamine at 550 °C for 4 h. The synthesized samples were investigated by X-ray diffraction (XRD), Fourier transform infrared (FT-IR), scanning electron microscopy (SEM), and photoluminescence (PL) techniques, which confirms their successful fabrication (Figures S1−S5). The details of the characterizations can be found in the Supporting Information.

2.2. Photocatalytic Inactivation of Marine Bacteria. The bacterial inactivation experiments were conducted in seawaters that were collected from Pearl River Estuary and filtered by a 0.22 μm filter before use. The salinity of seawaters was approximately 28.8‰. The detailed water quality index is shown in Table S1. *V. alginolyticus* was used as the marine bacterial indicator for ballast water treatment according to a previous report.[27] The *V. alginolyticus* cells were cultured in fluid 2216E media at 37 °C while being shaken for 20 h. The harvested bacteria were washed three times with sterilized saline (0.9% NaCl), followed by resuspension in sterilized seawater. Then, 50 mg of g-C_3N_4/PDI and a certain amount of Fe(II) ($FeSO_4·7H_2O$, Aldrich, 99%) were dispersed into 50 mL of bacterium-containing seawater (10^7 CFU/mL) and kept in the dark for 30 min before being irradiated. The system was then illuminated using a 300 W xenon lamp equipped with a 420 nm cutoff filter. The light intensity for VL irradiation was kept at 60 mW/cm^2. At a fixed interval, the samples were collected and serially diluted with sterile seawater. Then, a 0.1 mL sample dilution was promptly spread on 2216E agar plates to identify the viable cells. All of the experiments described above were performed three times.

2.3. Analysis. The concentration of photogenerated H_2O_2 was determined by the DPD/POD method,[28] and detailed information can be found in the Supporting Information. The production of •OH was studied by the method of photoluminescence with coumarin (excitation at 332 nm, emission at 460 nm).[29] Intracellular levels of reactive oxygen species (ROS) were analyzed by a Reactive Oxygen Species Assay Kit using fluorogeic dye 2′,7′-dichlorofluorescein diacetate (DCFH-DA) (S0033, Boyotime).[30,31] The Bacterial Protein Extraction Kit (C600596, Sangon Biotech) was used to extract intracellular enzyme proteins, and then the Modified Bradford Protein Assay Kit (C503041, Sangon Biotech) and the

https://doi.org/10.1021/acsestwater.1c00048
ACS EST Water 2021, 1, 1483−1494

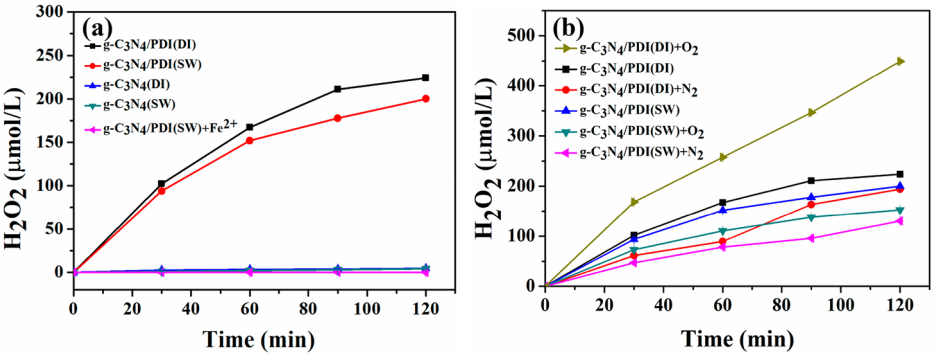

Figure 1. (a) Comparison of photocatalytic H_2O_2 production in deionized water (DI) and seawater (SW) using g-C_3N_4 and g-C_3N_4/PDI as the photocatalysts (or with the addition of 1.8 mM Fe^{2+}). (b) Photocatalytic H_2O_2 production over g-C_3N_4/PDI in DI and SW under air, N_2, and O_2-saturated conditions. Experimental conditions: 1.0 g/L catalyst, $\lambda \geq 420$ nm, T = 30 °C, $[pH]_0$ = 8.1.

Catalase Assay Kit (S0051, Boyotime) were used to determine the protein concentration and CAT activity, respectively. The changes in the morphology of the bacteria during inactivation were studied by SEM (Hitachi SU8200), and the detailed SEM sample preparation protocol is outlined in the Supporting Information. The dissolved oxygen concentrations in seawater and deionized water were measured by a dissolved oxygen meter (ST300D, OHAUS). The concentration of dissolved organic carbon was measured by a total organic carbon analyzer (TOC VCPH, Shimadzu). Samples were collected from the reaction medium and filtered with a 0.45 μm membrane before analysis. The three-dimensional excitation−emission matrix (EEM) spectrum of the sample was obtained using a fluorescence spectrometer (FLS1000). The excitation wavelength was scanned from 220 to 500 nm, and the emission wavelength was scanned from 300 to 500 nm. Parallel factor analysis (PARAFAC) of EEM data for all samples was conducted using the DOMFluor toolbox in Matlab according to the method of Stedmon and Bor.[29]

Acute toxicity was tested with bioluminescent bacterium *Vibrio fischeri* as the subject organism. Samples were mixed with a *V. fischeri* suspension for a 15 min incubation, which was then tested by a DXY-3 toxicity analyzer (Nanjing Quark Technology). *V. fischeri* incubated in seawater without catalysts was used as the control group. The acute toxicity was estimated by the inhibition ratio (IR) of bioluminescence, which was calculated with the equation IR = $(I_c - I_s)/I_c$, where I_c and I_s are the bioluminescence intensities of the control group and sample solutions, respectively. The variations of the inorganic ion concentration during the reaction were also measured by inductively coupled plasma mass spectrometry (ICP-MS) (Thermo Fisher, ICAP RQ).

3. RESULTS AND DISCUSSION

3.1. Photocatalytic Production of H_2O_2. Understanding photocatalytic H_2O_2 production performance in aqueous medium under VL irradiation is an essential prerequisite for constructing the *in situ* photo-Fenton system, especially in a seawater system. Therefore, the H_2O_2 production efficiency in deionized water and seawater was compared. Figure 1a shows that very little H_2O_2 was produced by pristine g-C_3N_4 in both deionized water and seawater (~4 μmol/L). In contrast, g-C_3N_4/PDI can produce 223.9 μmol of H_2O_2/L in deionized water within 120 min of VL illumination, which is noticeably 50 times higher than that of bare g-C_3N_4. This could be attributed to the results showing that the introduction of PDI units into g-C_3N_4 frameworks could promote the VL absorption capacity (Figure S2) and improve the charge transfer efficiency, as confirmed by the deceased PL intensity (Figure S4) and fluorescence decay lifetime (Figure S5). It was also interesting to find that H_2O_2 production still reached 199.9 μmol/L in seawater, which was similar to or only slightly lower than that in deionized water. The slightly lower H_2O_2 production efficiency may be due to the difference in dissolved oxygen in seawater and deionized water. The dissolved oxygen concentrations in seawater and deionized water were measured to be 5.3 and 8.1 mg/L, respectively. Therefore, the dissolved oxygen concentration in seawater was lower than that of deionized water, resulting in the slightly lower H_2O_2 production activity. The efficiency of solar-to-chemical conversion (SCC) for H_2O_2 production in seawater was calculated to be 0.1%, which was also similar to that in a deionized water system (Figure S6) and consistent with a previous study.[32] In seawater, although organic and inorganic substances were supposed to inhibit the photocatalytic reaction, some ions such as Cl^- were also reported to act as h^+ trapping agents to promote H_2O_2 production,[33] because the efficient trapping of h^+ prevented h^+−e^- recombination; thus, more e^- could be used for H_2O_2 production via the O_2 reduction pathway. The compromise of positive and negative effects led to H_2O_2 production not being significantly affected by the seawater/marine environment. The H_2O_2 concentration in the system decreased to almost zero with the addition of Fe(II), which indicates that the produced H_2O_2 can be promptly activated by Fenton reactions and decomposed for subsequent marine bacterial inactivation applications.

The influence of dissolved O_2 on the production efficiency of H_2O_2 was further studied. Figure 1b demonstrates that the H_2O_2 yield in deionized water increases dramatically to 449.3 μmol/L under O_2 bubbling conditions with an increase in SCC to 0.12% (Figure S6) and decreases significantly under N_2 bubbling conditions. This further confirms that H_2O_2 production follows the photogenerated e^--mediated O_2 reduction pathway, because increasing the level of dissolved O_2 can improve the reaction efficiency.[23] Therefore, dissolved O_2 has a strong influence on the production of H_2O_2 in deionized water. However, the produced H_2O_2 concentrations in seawater under O_2 bubbling, air equilibrium, and N_2 bubbling conditions were almost similar, suggesting the dissolved O_2 had a much weaker influence on H_2O_2 production in seawater than in deionized water, which also indicates that the seawater has a buffering effect on H_2O_2

https://doi.org/10.1021/acsestwater.1c00048
ACS EST Water 2021, 1, 1483−1494

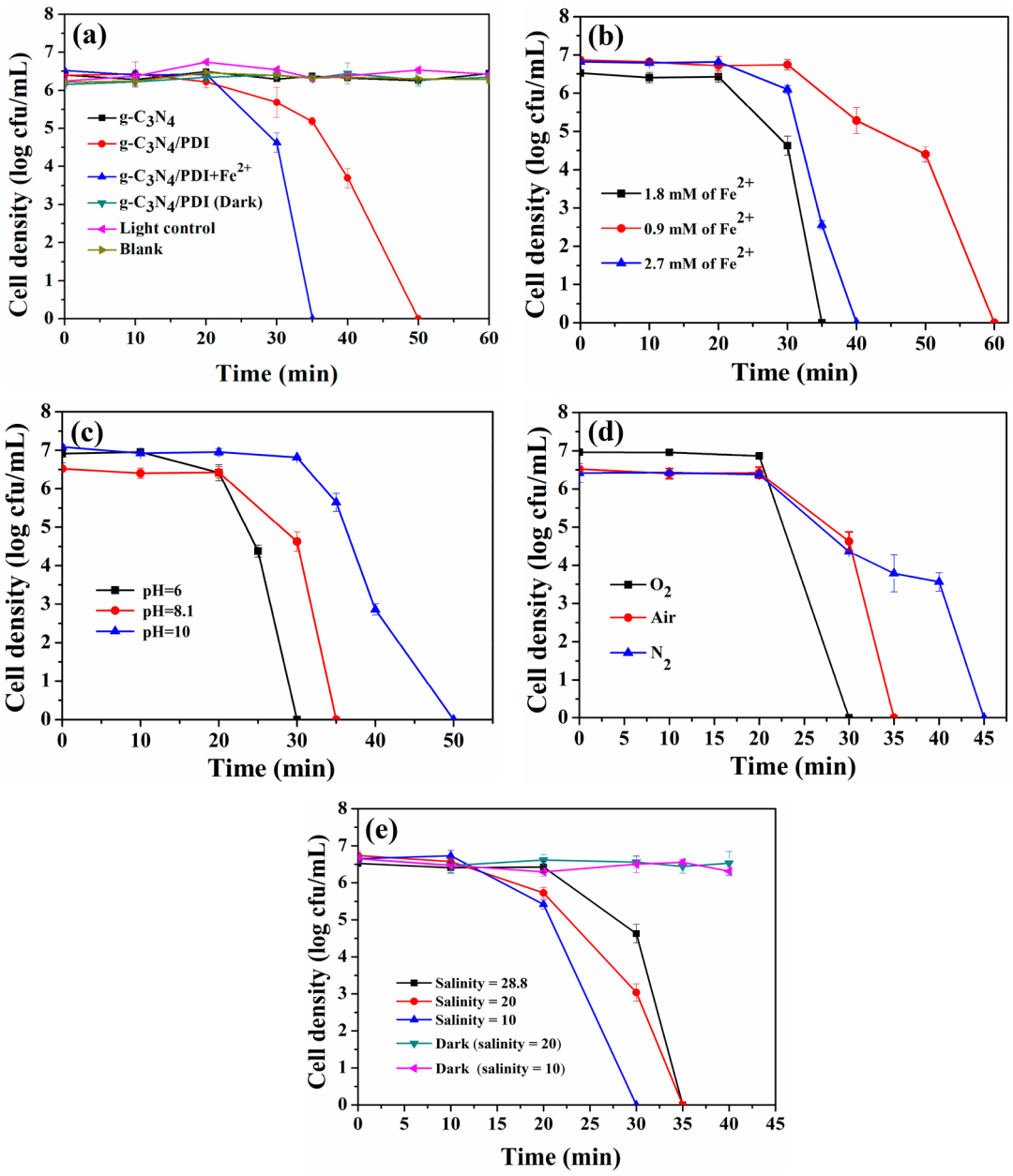

Figure 2. (a) *In situ* photo-Fenton inactivation of *V. alginolyticus* in g-C_3N_4, g-C_3N_4/PDI, and g-C_3N_4/PDI/Fe^{2+} systems. (b) Effect of Fe^{2+} concentration, (c) pH, (d) atmosphere, and (e) salinity on the bacterial inactivation efficiency in the g-C_3N_4/PDI/Fe^{2+} system. Experimental conditions: cell density of 7 log CFU/mL, 1.0 g/L catalyst, $\lambda \geq 420$ nm, T = 30 °C, $[pH]_0$ = 8.1.

production. Because the influence of dissolved O_2 was not significant, this system showed potential to be applied under both aerobic and anaerobic conditions, exhibiting a wide application value. It was also interesting to find that even in the presence of N_2 purging, g-C_3N_4/PDI could still produce >100 μM H_2O_2, which might be derived from two-electron water oxidation by photogenerated holes. The introduction of PDI units into g-C_3N_4 frameworks could positively shift the position of VB and increase the oxidation capacity, resulting in an increase in H_2O_2 production efficiency.[23,34]

3.2. *In Situ* Photo-Fenton Inactivation of Bacteria. *V. alginolyticus* was the most dominant pathogenic bacterium in ballast water, which needs to be strictly restricted according to the Ballast Water Management Convention (BWMC) guidelines.[35] Therefore, the bacterial inactivation activity was tested using *V. alginolyticus* as a model species in seawater under VL irradiation. Pristine g-C_3N_4 had no photocatalytic inactivation effect on *V. alginolyticus*, while ~6.5 log of *V. alginolyticus* was inactivated within 60 min by using PDI-modified g-C_3N_4 (Figure 2a). This was obviously due to the enhanced production of H_2O_2, because the H_2O_2 can act as a germicide and predominant species in photocatalytic bacterial inactivation processes.[36] Interestingly, with the incorporation of Fe^{2+}, the inactivation efficiency was further improved remarkably and total inactivation of all *V. alginolyticus* was achieved within 35 min of VL irradiation. It has been reported that an electrochemical method for inactivation of *V. alginolyticus* could achieve only 3.0 log reduction within 1 h.[37] Other advanced oxidation technologies, such as UV/O_3, UV/Ag-TiO_2, and UV/Ag-TiO_2/O_3, were able to inactivate 5.0 log *V. alginolyticus* within 5 min.[27] However, these systems can operate under UV irradiation only with the addition of strong

https://doi.org/10.1021/acsestwater.1c00048
ACS EST Water 2021, 1, 1483−1494

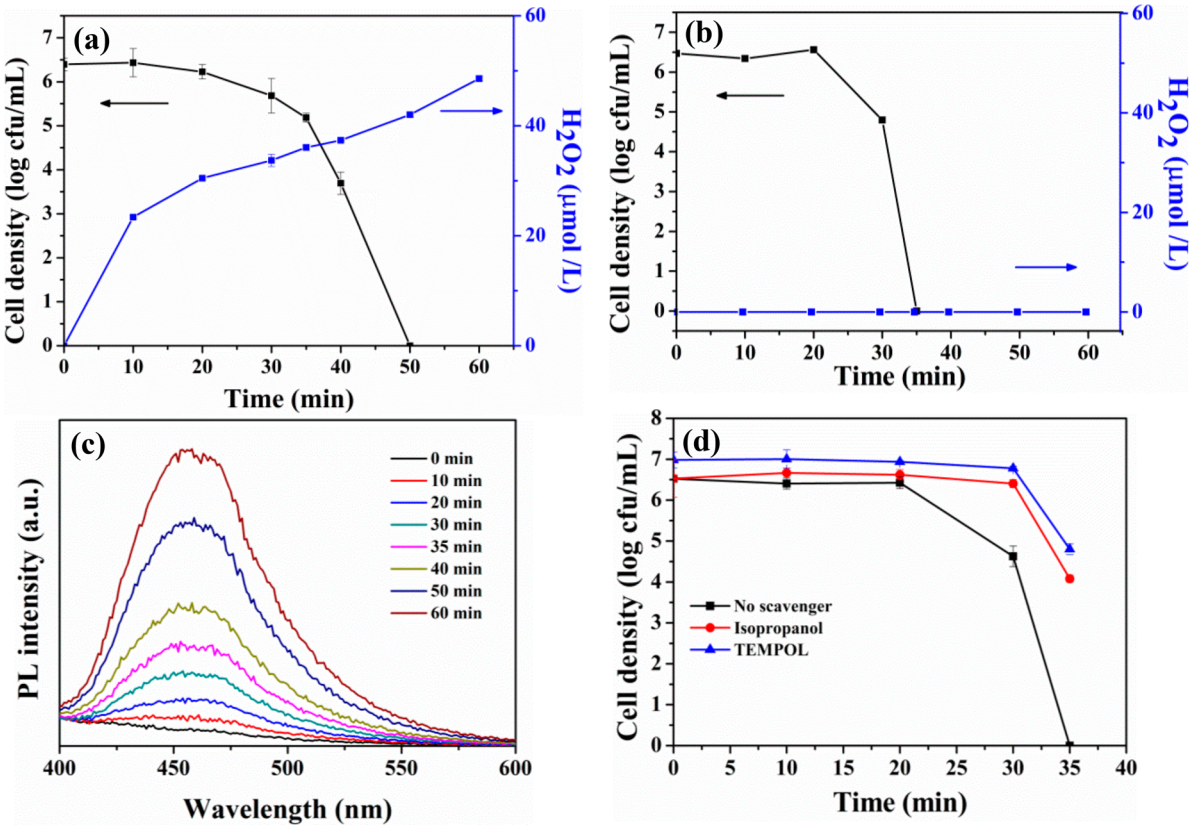

Figure 3. Simultaneous monitoring of bacterial inactivation and the *in situ*-generated H_2O_2 concentration in (a) g-C_3N_4/PDI and (b) g-C_3N_4/PDI/Fe^{2+} systems. (c) Fluorescence spectra of a coumarin solution (1 mM) in the g-C_3N_4/PDI/Fe^{2+} system. (d) *V. alginolyticus* inactivation efficiency with different scavengers (0.5 mmol/L isopropanol and 0.1 mmol/L TEMPOL). Experimental conditions: cell density of 7 log CFU/mL, 1.0 g/L catalyst, $[Fe^{2+}]$ = 1.8 mM, $\lambda \geq 420$ nm, T = 30 °C, $[pH]_0$ = 8.1.

oxidants (i.e., O_3), which is costly and energy intensive. In addition, the achieved bacterial inactivation performance in the g-C_3N_4/PDI/Fe^{2+} system was higher than those of almost all of the g-C_3N_4-based photocatalysts reported so far (Table S2). It was noted that existing studies have validated the effective inactivation of freshwater bacteria (e.g., *E. coli*) by g-C_3N_4-based photocatalysts.[38,39] However, in this study, pristine g-C_3N_4 had a negligible inactivation effect on *V. alginolyticus*, suggesting inactivation of marine bacteria in seawater was much more difficult. This result indicates the *in situ* photo-Fenton system shows promise for marine bacterial inactivation in seawater.

The relationships between bacterial inactivation efficiency and several operation factors were also investigated. For the effect of Fe^{2+} dosage, it was found that the bacterial inactivation performance was first increased with an increase in Fe^{2+} concentration from 0.9 to 1.8 mM and then decreased when the Fe^{2+} concentration further increased to 2.7 mM (Figure 2b). The highest inactivation efficiency was obtained with an Fe^{2+} concentration of ∼1.8 mM. The decrease in inactivation efficiency at high Fe^{2+} dosage was probably due to the fact that excess Fe^{2+} could react with •OH to form Fe^{3+} and OH^-, which consumes •OH thus leading to the decrease in the oxidation capacity of the Fenton system.[40−42] To further study the pH effect, the reaction was first carried out under natural seawater conditions (pH 8.1) without pH adjustment. Then, comparative experiments were also performed by adjusting the pH using dilute HCl and NaOH solutions. As shown in Figure 2c, the inactivation efficiency was improved with a decrease in pH, while a high efficiency was maintained when the pH was increased to 10, suggesting pH is an important experimental parameter that influences the disinfection efficiency. Traditional homogeneous Fenton systems are operated under acidic conditions, and pH preconditioning is usually required.[43] In contrast, the *in situ* photo-Fenton system presented here can be operated in alkaline seawater without the need for pH preadjustment.

The sterilization effect could be further improved with the introduction of O_2 and inhibited with N_2 aeration (Figure 2d). Given that the H_2O_2 production efficiency was not significantly affected by dissolved O_2, the improvement in sterilization efficiency may be attributed to the enhanced production of other ROS, such as $\bullet O_2^-$, which will be verified by subsequent scavenging experiments (see Figure 3d). In general, complete inactivation of *V. alginolyticus* was reached within 30−45 min under different gas bubbling conditions, suggesting the influence of aerobic or anaerobic conditions on the inactivation efficiency in this new photo-Fenton system was not significant. To further investigate the effect of salinity, the experiments were conducted in seawater with different salinities (10−28.8‰). The results show that the inactivation was gradually inhibited by an increase in salinity (Figure 2e), suggesting salinity might be the major factor in defining the bacterial inactivation efficiency. To further study the effect of Cl^- (major ions in seawater), additional experiments were conducted in a saline solution prepared with only NaCl with the same salinity as natural seawater (28.8‰). The results demonstrated that *V. alginolyticus* inactivation was significantly

https://doi.org/10.1021/acsestwater.1c00048
ACS EST Water 2021, 1, 1483−1494

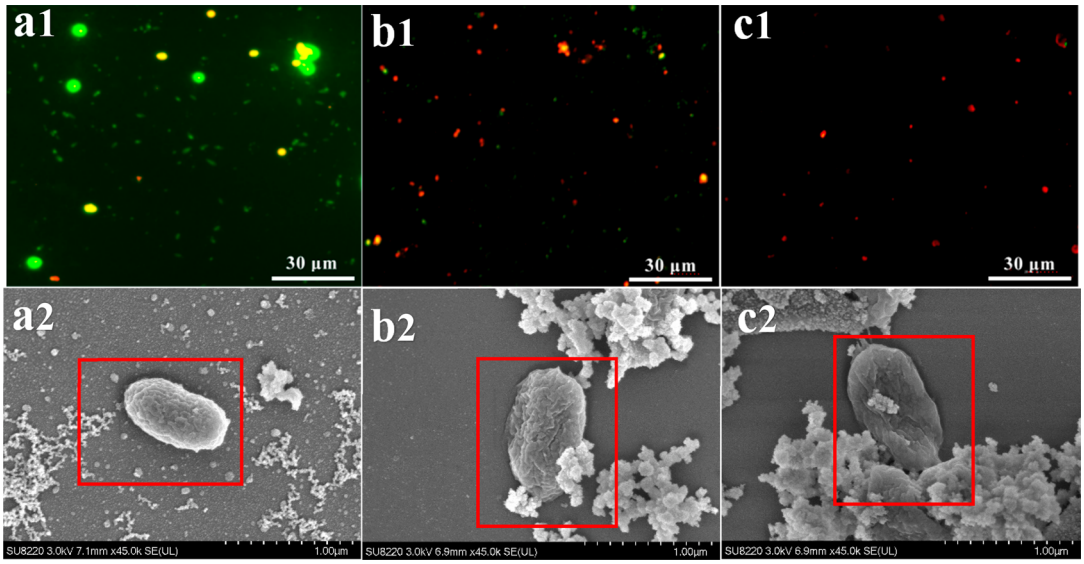

Figure 4. Fluorescence microscopic images and scanning electron microscopy (SEM) images of *V. alginolyticus* cells treated by the g-C_3N_4/PDI/Fe^{2+} system with different VL irradiation times: (a1 and a2) 0 min, (b1 and b2) 20 min, and (c1 and c2) 30 min. Experimental conditions: cell density of 7 log cfu/mL, 1.0 g/L catalyst, $[Fe^{2+}]$ = 1.8 mM, $\lambda \geq 420$ nm, T = 30 °C, $[pH]_0$ = 8.1.

enhanced, as the bacterial cells could be completely inactivated in only 15 min (Figure S7), indicating the salinity with Cl^- was not the major inhibitory factor. These results indicate that natural seawater contained micronutrients rather than Cl^- that can "protect" the bacterial cells from external oxidation damage, making the sterilization much more difficult in seawater than in freshwater even with the same salinity.

3.3. Roles of Reactive Species. To double confirm the *in situ* coupling mechanism and study the role of reactive species, the relationship between H_2O_2 production and bacterial inactivation was studied by simultaneously monitoring the bactericidal activity and H_2O_2 production. In the g-C_3N_4/PDI system, the complete inactivation of *V. alginolyticus* was observed within 50 min, while H_2O_2 production gradually increased to 48.9 μmol/L in the meantime (Figure 3a). After the addition of Fe^{2+} as an activator, although the inactivation efficiency was greatly improved, H_2O_2 production was not detected in the g-C_3N_4/PDI/Fe^{2+} system (Figure 3b). This suggests the improvement of bactericidal activity is caused by the *in situ* activation of H_2O_2 to produce •OH, instead of the H_2O_2 itself. To verify this point, control experiments were conducted by directly adding a H_2O_2 solution to test the disinfection in the seawater environment and it was found that the H_2O_2 concentration needed to reach 400 μmol/L to achieve a significant sterilization effect (Figure S8), which far exceeded the amount of H_2O_2 produced by g-C_3N_4/PDI within the test period of 60 min. Therefore, H_2O_2 was not the reason for the high sterilization efficiency in this system; instead, the •OH produced by Fe^{2+}-triggered Fenton reaction should be the major reactive species.

To further verify that H_2O_2 was activated *in situ*, coumarin was used as a captor to monitor •OH production, because coumarin can react with •OH to generate 7-hydroxycoumarin that has sensitive fluorescence properties.[44−46] As shown in Figure 3c, the fluorescence intensity of 7-hydroxycoumarin increased with irradiation time, indicating H_2O_2 was successfully activated; thus, •OH was generated under VL irradiation. To further study whether the bacterial inactivation was caused by •OH, scavengers were used to suppress the •OH-mediated processes during photocatalytic inactivation of *V. alginolyticus*, employing isopropanol for •OH[47] and TEMPOL (1-λ1-oxidanyl-2,2,6,6-tetramethylpiperidin-4-ol) for $•O_2^-$.[48] As shown in Figure 3d, the inactivation efficiency was significantly inhibited upon the addition of isopropanol, and an only 2.5 log reduction of *V. alginolyticus* was obtained within 35 min, suggesting that •OH was involved in the process of bacterial inactivation. With the addition of TEMPOL to quench $•O_2^-$, the inactivation efficiency was further inhibited (only 2.1 log reduction within 35 min), which could be attributed to two reasons. (1) $•O_2^-$ was reported to be the precursor for H_2O_2 production;[34] thus, the quenching of $•O_2^-$ would lead to a decrease in the levels of H_2O_2 and •OH. (2) $•O_2^-$ could be also directly involved in *V. alginolyticus* inactivation, which is supported by a previous study in which $•O_2^-$ can directly inactivate *E. coli* cells.[48] In general, in the *in situ* photo-Fenton system presented here, the H_2O_2 was produced by the photocatalyst (i.e., g-C_3N_4/PDI). The produced H_2O_2 was activated *in situ* by Fe(II) to generate •OH, which was responsible for the inactivation of *V. alginolyticus* cells. Therefore, no external oxidants (i.e., H_2O_2) were required, while for traditional advanced oxidation processes, external oxidants were needed to trigger the reactions.

3.4. Bacterial Inactivation Mechanism. The in-depth exploration of the bacterial inactivation mechanism is vitally important to develop effective disinfection methods; thus, the ballast water bacterial inactivation mechanism and processes by the *in situ* photo-Fenton system were further studied. The bacterial cell envelope might be the first attacking sites during bacterial inactivation by ROS. Thus, the bacterial cell membrane integrity was visually studied through a SYTO 9/PI fluorescence assay as reported in ref 49. SYTO 9 is a green fluorescence and membrane permeable dye for nucleic acid staining in live bacteria, while PI can enter only through a damaged bacterial membrane, which can quench SYTO 9 emission, producing red fluorescence to locate dead bacteria. It was found that in addition to the orange-yellow fluorescence from the catalyst, bacterial cells at the initial stage showed

https://doi.org/10.1021/acsestwater.1c00048
ACS EST Water 2021, 1, 1483−1494

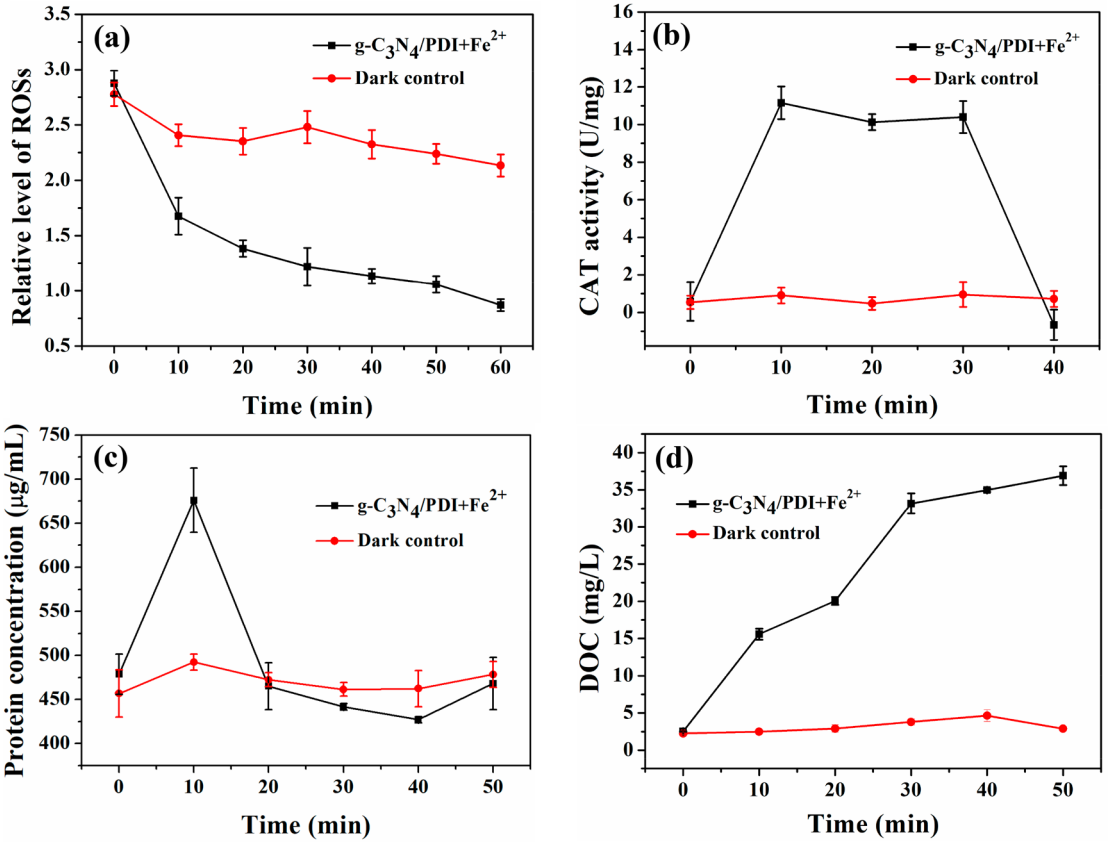

Figure 5. (a) Intracellular ROS levels, (b) catalase (CAT) activity, (c) total protein contents, and (d) released dissolved organic carbon (DOC) concentration during the *V. alginolyticus* inactivation process in the *in situ* photo-Fenton system. Experimental conditions: cell density of 7 log CFU/mL, 1.0 g/L catalyst, $\lambda \geq 420$ nm, T = 30 °C, $[pH]_0$ = 8.1.

green fluorescence (Figure 4a1), suggesting the cell membrane was intact at the beginning. After treatment for 20 min, the number of red fluorescent cells increased (Figure 4b1). Finally, almost all of the cells became red after treatment for 30 min (Figure 4c1), suggesting that the cell membrane was ruptured and the cell lysis efficiency reached almost 100% after the inactivation treatment. The morphology changes of *V. alginolyticus* during the inactivation were further investigated by SEM. Obviously, untreated *V. alginolyticus* formed plump rod shapes (Figure 4a2). After light irradiation for 20 min, the cell membrane began to wrinkle and pores appeared (Figure 4b2). Finally, the cell membrane was severely damaged, and the cells were mostly concave after treatment for 30 min (Figure 4c2). Because cell metabolism occurs on the cell membrane in prokaryotes, the disruption of the cell membrane results in metabolic arrest, leading to cell death.[50]

Meanwhile, endogenous damage caused by oxidative stress (intracellular ROS) may also result in bacterial inactivation.[31] To verify this assumption, fluorescent probe DCFH-DA was used to detect the intracellular ROS level. After the DCFH-DA entered the cell, its enzymatic hydrolysis product, DCFH, could not be released if the cell membrane remained intact. It was found that the intracellular ROS level decreased remarkably with reaction time (Figure 5a), suggesting the intracellular oxidative stress was released due to the damage to the membrane. This result also indicates that rapid and massive •OH generated in this system oxidizes cell membranes promptly, causing bacteria to die before generating intracellular oxidative stress. To further confirm this claim, the activity of CAT was also tested. The results show that the CAT activity was increased promptly in the first 10 min and then decreased thereafter (Figure 5b), which is generally consistent with the trend of the intracellular ROS level. The initial increase in CAT activity indicates the cells were also subjected to H_2O_2 stress at the beginning of the *in situ* Fenton reaction, which doubly confirms that the first event in this system is generation of H_2O_2, leading to upregulation of intracellular oxidative stress, followed by activation of H_2O_2 to produce •OH causing subsequent complete destruction of the cells.

The destruction processes were then studied by monitoring the changes in total soluble protein and dissolved organic carbon. The initial concentration of the total protein is 478 μmol/L, which originated from cell metabolism. With continuous treatment, the protein concentration increased quickly and reached the highest value (667 μmol/L) within 10 min of VL irradiation (Figure 5c), which can be ascribed to cell membrane damage leading to intracellular protein efflux. Thereafter, the protein concentration began to decrease, suggesting the intracellular proteins, including antioxidant enzymes, were overwhelmed and degraded by ROS attacking.[51] In addition, damage to the cell membrane could also lead to the loss of membrane-associated protein.[52] Moreover, dissolved organic carbon (DOC) was also monitored during the bacterial inactivation process, and the concentration continued to increase as the reaction progressed within 60 min (Figure 5d), which provides additional evidence that the inactivation process destroys the cell membrane, causing the release of biomacromolecule organics into the external

https://doi.org/10.1021/acsestwater.1c00048
ACS EST Water 2021, 1, 1483−1494

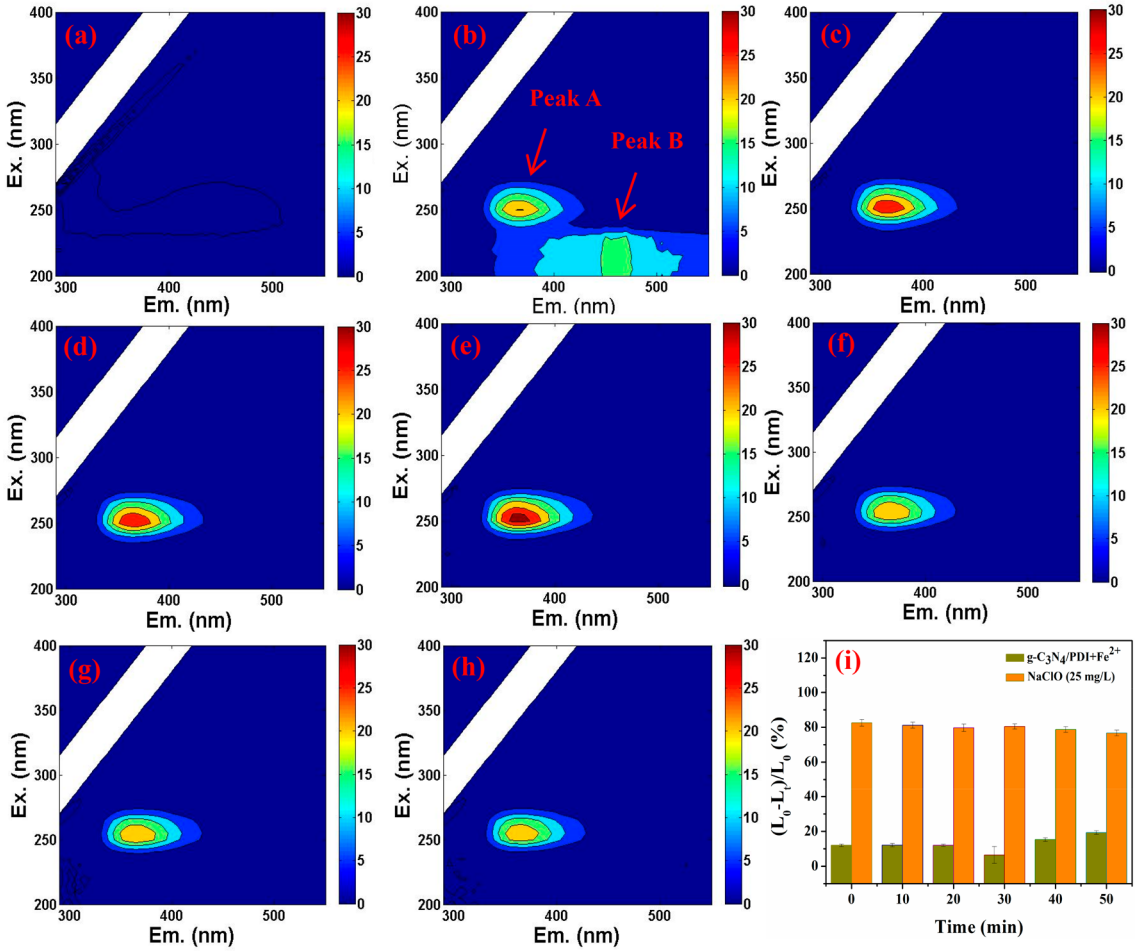

Figure 6. Contour plots of the components identified from the complete EEM data sets treated by the g-C_3N_4/PDI/Fe^{2+} system with different irradiation times: (a) raw seawater and (b) 0, (c) 10, (d) 20, (e) 30, (f) 40, (g) 50, (h) 60 min. (i) Percent luminous intensity of *V. fischeri* during photocatalytic inactivation. Experimental conditions: cell density of 7 log CFU/mL, 1.0 g/L catalyst, $\lambda \geq 420$ nm, T = 30 °C, $[pH]_0$ = 8.1.

environment. It should be noted that although macromolecules such as protein can be degraded, the complete mineralization of intracellular organic molecules is not reached completely, probably due to the short treatment time. This phenomenon has also been found in previous photocatalytic bacterial inactivation systems.[53,54]

3.5. Evolution of Toxicity during the Release of Residues. To understand the impact of released organic matter on the water environment after photocatalytic treatment by the *in situ* photo-Fenton system, fluorescence EEM combined with PARAFAC was used to characterize the release profiles during bacterial inactivation. Figure 6a depicts that there was no fluorescence of sterile seawater used in the experiments, excluding the possible background EEM signals from seawater. After the addition of *V. alginolyticus* and catalysts with a 30 min dark incubation, two distinct peaks at excitation and emission wavelengths of 250 and 365 nm, respectively (peak A), and 220 and 460 nm, respectively (peak B), appeared (Figure 6b). According to previous studies, fluorescent peak A can be assigned to tryptophan-like proteins.[55−57] It was noticed that the intensity of peak A increased gradually in the first 30 min and then decreased thereafter (Figure 6b−h). This trend is consistent with the protein concentration change mentioned above (Figure 5c), suggesting tryptophan-like proteins were really released as a result of membrane rupture, which could be further decomposed by •OH. Fluorescent peak B was reported to arise from pteridine compounds, which are believed to be cell metabolites widely presented in bacteria according to ref 58. Upon treatment for 10 min, fluorescent peak B rapidly decreased and became completely disappeared within 10 min (Figure 6b−h), suggesting that the bacterial metabolites could also be degraded in this system.

The changes in major seawater quality parameters were also monitored during the inactivation process (Table S1). The sterilization experiments were conducted in seawater without buffer solutions. The initial pH of bacterium-contaminated seawater was determined to be 8.1, which decreased to 3.96 after the *in situ* photo-Fenton treatment for 40 min. As the pH value decreases, the level of the photoactive iron complex $Fe(OH)^{2+}$ increases, thereby accelerating the inactivation of bacteria. In addition, the K^+ concentration was observed to be significantly increased by ∼8.24 times, which is another indicator of cell membrane damage resulting in leakage of K^+.[59] Those of other ions, including Na^+, Ca^{2+}, Mg^{2+}, Cl^-, SO_4^{2-}, and Br^-, were not changed significantly or only slightly increased, probably due to water evaporation during the treatment process. The inorganic ions may be adsorbed on the cells to form a protective layer, thus preventing the bacteria from ROS attacking.[60] Natural seawater contains many inorganic ions and organic ions, so it is difficult to predict the interaction of various ions in this system. Even so, the

https://doi.org/10.1021/acsestwater.1c00048
ACS EST Water 2021, 1, 1483−1494

present g-C_3N_4/PDI/Fe^{2+} photo-Fenton system is effective for the sterilization in seawater under visible light illumination.

To further assess the impact of possible released disinfection byproducts on this sterilization method in the marine water environment, the acute toxicity of the filtered reaction medium was evaluated using luminescent bacterium *V. fischeri* as a probe according to the methodology in ref 61. The inhibition of the bioluminescence of *V. fischeri* upon exposure to a toxicant can be used to indicate the acute toxicity. The traditional sodium hypochlorite disinfection method was used as a control.[62] Figure 6i shows the relative percentage inhibition of luminescent bacteria incubated with a filtered reaction solution during different treatment times. Obviously, the IR of luminescent bacteria after inactivation treatment by the g-C_3N_4/PDI/Fe^{2+} system remains below 20%. However, when sodium hypochlorite was used for the inactivation, the luminescent bacteria are inhibited by >80%, suggesting the effluents of the traditional sodium hypochlorite inactivation method are highly toxic to the marine environment. These results further confirm that the g-C_3N_4/PDI/Fe^{2+} *in situ* photo-Fenton inactivation technology is green and environmentally friendly with the inactivation effluents having low cytotoxicity.

4. CONCLUSIONS

Current ballast water sterilization technologies are mostly based on consuming-type chemical oxidants (i.e., halogenated disinfectants, peroxides, and persulfates) or require a large amount of energy (i.e., UV irradiation and electrochemical methods). This study provides a new *in situ* photo-Fenton system for marine bacterial inactivation in seawater. g-C_3N_4/PDI was utilized as a model photocatalyst to produce H_2O_2, which was activated *in situ* by Fe(II) to produce •OH for bacterial inactivation. *V. alginolyticus* (7 log) in ballast seawater could be totally inactivated within 35 min of VL irradiation. The proposed *in situ* photo-Fenton system can compete in at least four aspects. (i) The oxidants are continuously generated *in situ* by photocatalysis; thus, no external disinfectants (i.e., H_2O_2) are required. The mode of spontaneous generation of oxidants is also superior to the sequential batch addition mode of oxidants, which would further reduce the costs of operation. (ii) The system is active under VL irradiation, avoiding the use of high-intensity UV lamp irradiation. Thus, on-board treatment can be realized using the abundant sunlight energy at sea, which fulfills the requirements of sustainable development. (iii) Compared with a traditional Fenton system in which an acidic condition is required, the system presented here can be operated directly in alkaline seawater without the need for pH preadjustment. (iv) The possible released organic matter and disinfection byproducts have minimal toxicity and a weaker impact on the marine water environment. In addition to the advantage of using sunlight as the energy source, the g-C_3N_4 catalyst is also inexpensive and environmentally friendly. The system does not require additional H_2O_2 or other oxidants compared to the ordinary Fenton method. Therefore, this technology shows advantages in various aspects of energy conservation. More generally, the system that can be further promoted by changing high-efficiency H_2O_2 production photocatalysts and assembled with Fenton catalysts for consolidation is versatile. In addition, mechanistic insights regarding bacterial inactivation processes in terms of cell membrane rapture, intracellular enzyme activity, total protein changes, and intracellular release profiles were clarified, which will provide additional insights for exploring marine bacterial inactivation mechanisms in seawater.

■ ASSOCIATED CONTENT

Supporting Information

The Supporting Information is available free of charge at https://pubs.acs.org/doi/10.1021/acsestwater.1c00048.

Experimental details (characterization of materials, measurement of produced H_2O_2, SCC efficiency calculation, and bacterial sample preparation protocol for SEM observation); XRD, FT-IR, UV−vis DRS, SEM, TEM, and photoluminescence spectra; time-resolved fluorescence decay spectra of the g-C_3N_4 and g-C_3N_4/PDI samples; SCC efficiency for photocatalytic H_2O_2 production; inactivation efficiency in a NaCl solution; inactivation efficiency with the addition of only H_2O_2; comparison of the bacterial inactivation efficiency with other g-C_3N_4 photocatalytic systems; and changes in seawater quality parameters during the treatment process (PDF)

■ AUTHOR INFORMATION

Corresponding Author

Taicheng An − *Guangdong Key Laboratory of Environmental Catalysis and Health Risk Control, Guangdong Hong Kong-Macao Joint Laboratory for Contaminants Exposure and Health, Institute of Environmental Health and Pollution Control and Guangzhou Key Laboratory Environmental Catalysis and Pollution Control, Key Laboratory of City Cluster Environmental Safety and Green Development, School of Environmental Science and Engineering, Guangdong University of Technology, Guangzhou 510006, China;* orcid.org/0000-0001-6918-8070; Phone: +86 20 3932 2298; Email: antc99@gdut.edu.cn; Fax: +86 20 3932 2298

Authors

Wanjun Wang − *Guangdong Key Laboratory of Environmental Catalysis and Health Risk Control, Guangdong Hong Kong-Macao Joint Laboratory for Contaminants Exposure and Health, Institute of Environmental Health and Pollution Control and Guangzhou Key Laboratory Environmental Catalysis and Pollution Control, Key Laboratory of City Cluster Environmental Safety and Green Development, School of Environmental Science and Engineering, Guangdong University of Technology, Guangzhou 510006, China;* orcid.org/0000-0003-1193-1030

Haojing Xie − *Guangdong Key Laboratory of Environmental Catalysis and Health Risk Control, Guangdong Hong Kong-Macao Joint Laboratory for Contaminants Exposure and Health, Institute of Environmental Health and Pollution Control, Guangdong University of Technology, Guangzhou 510006, China*

Guiying Li − *Guangdong Key Laboratory of Environmental Catalysis and Health Risk Control, Guangdong Hong Kong-Macao Joint Laboratory for Contaminants Exposure and Health, Institute of Environmental Health and Pollution Control and Guangzhou Key Laboratory Environmental Catalysis and Pollution Control, Key Laboratory of City Cluster Environmental Safety and Green Development, School of Environmental Science and Engineering,*

Guangdong University of Technology, Guangzhou 510006, China; orcid.org/0000-0002-6777-4786

Jia Li − *Guangdong Key Laboratory of Environmental Catalysis and Health Risk Control, Guangdong Hong Kong-Macao Joint Laboratory for Contaminants Exposure and Health, Institute of Environmental Health and Pollution Control, Guangdong University of Technology, Guangzhou 510006, China*

Po Keung Wong − *Guangdong Key Laboratory of Environmental Catalysis and Health Risk Control, Guangdong Hong Kong-Macao Joint Laboratory for Contaminants Exposure and Health, Institute of Environmental Health and Pollution Control and Guangzhou Key Laboratory Environmental Catalysis and Pollution Control, Key Laboratory of City Cluster Environmental Safety and Green Development, School of Environmental Science and Engineering, Guangdong University of Technology, Guangzhou 510006, China;* orcid.org/0000-0003-3081-960X

Complete contact information is available at: https://pubs.acs.org/10.1021/acsestwater.1c00048

Notes

The authors declare no competing financial interest.

■ ACKNOWLEDGMENTS

This work was supported by the Science and Technology Program of Guangzhou, China (202002030177), the Guangdong Basic and Applied Basic Research Foundation for Distinguished Young Scholars (2021B1515020063), the National Natural Science Foundation of China (21607028 and U1901210), the National Key Research and Development Program of China (2019YFC1804501), the Local Innovative and Research Teams Project of Guangdong Pearl River Talents Program (2017BT01Z032), and the Guangdong Provincial Key R&D Program (2020B1111350002).

■ REFERENCES

(1) Nanayakkara, K. G.; Zheng, Y. M.; Alam, A. K.; Zou, S.; Chen, J. P. Electrochemical disinfection for ballast water management: technology development and risk assessment. *Mar. Pollut. Bull.* **2011**, *63*, 119−123.

(2) David, M.; Gollasch, S.; Cabrini, M.; Perkovic, M.; Bosnjak, D.; Virgilio, D. Results from the first ballast water sampling study in the Mediterranean Sea - the Port of Koper study. *Mar. Pollut. Bull.* **2007**, *54*, 53−65.

(3) La Carbona, S.; Viitasalo-Frosen, S.; Masson, D.; Sassi, J.; Pineau, S.; Lehtiniemi, M.; Corroler, D. Efficacy and environmental acceptability of two ballast water treatment chemicals and an alkylamine based-biocide. *Sci. Total Environ.* **2010**, *409*, 247−255.

(4) Lv, B. Y.; Cui, Y. X.; Tian, W.; Li, J.; Xie, B.; Yin, F. Abundances and profiles of antibiotic resistance genes as well as co-occurrences with human bacterial pathogens in ship ballast tank sediments from a shipyard in Jiangsu Province, China. *Ecotoxicol. Environ. Saf.* **2018**, *157*, 169−175.

(5) Lacasa, E.; Tsolaki, E.; Sbokou, Z.; Rodrigo, M. A.; Mantzavinos, D.; Diamadopoulos, E. Electrochemical disinfection of simulated ballast water on conductive diamond electrodes. *Chem. Eng. J.* **2013**, *223*, 516−523.

(6) Tsolaki, E.; Diamadopoulos, E. Technologies for ballast water treatment: a review. *J. Chem. Technol. Biotechnol.* **2010**, *85*, 19−32.

(7) Herwig, R. P.; Cordell, J. R.; Perrins, J. C.; Dinnel, P. A.; Gensemer, R. W.; Stubblefield, W. A.; Ruiz, G. M.; Kopp, J. A.; House, M. L.; Cooper, W. J. Ozone treatment of ballast water on the oil tanker S/T Tonsina: chemistry, biology and toxicity. *Mar. Ecol.: Prog. Ser.* **2006**, *324*, 37−55.

(8) Briski, E.; Gollasch, S.; David, M.; Linley, R. D.; Casas-Monroy, O.; Rajakaruna, H.; Bailey, S. A. Combining ballast water exchange and treatment to maximize prevention of species introductions to freshwater ecosystems. *Environ. Sci. Technol.* **2015**, *49*, 9566−9573.

(9) Hess-Erga, O.-K.; Blomvagnes-Bakke, B.; Vadstein, O. Recolonization by heterotrophic bacteria after UV irradiation or ozonation of seawater; a simulation of ballast water treatment. *Water Res.* **2010**, *44*, 5439−5449.

(10) Petersen, N. B.; Madsen, T.; Glaring, M. A.; Dobbs, F. C.; Jorgensen, N. O. G. Ballast water treatment and bacteria: Analysis of bacterial activity and diversity after treatment of simulated ballast water by electrochlorination and UV exposure. *Sci. Total Environ.* **2019**, *648*, 408−421.

(11) Wright, D. A.; Gensemer, R. W.; Mitchelmore, C. L.; Stubblefield, W. A.; van Genderen, E.; Dawson, R.; Orano-Dawson, C. E.; Bearr, J. S.; Mueller, R. A.; Cooper, W. J. Shipboard trials of an ozone-based ballast water treatment system. *Mar. Pollut. Bull.* **2010**, *60*, 1571−1583.

(12) Stehouwer, P. P.; Buma, A.; Peperzak, L. A comparison of six different ballast water treatment systems based on UV radiation, electrochlorination and chlorine dioxide. *Environ. Technol.* **2015**, *36*, 2094−2104.

(13) Bai, M. D.; Zheng, Q. L.; Tian, Y. P.; Zhang, Z. T.; Chen, C.; Cheng, C.; Meng, X. Y. Inactivation of invasive marine species in the process of conveying ballast water using center dot OH based on a strong ionization discharge. *Water Res.* **2016**, *96*, 217−224.

(14) Bai, M. D.; Tian, Y. P.; Yu, Y.; Zheng, Q. L.; Zhang, X. F.; Zheng, W.; Zhang, Z. T. Application of a hydroxyl-radical-based disinfection system for ballast water. *Chemosphere* **2018**, *208*, 541−549.

(15) Puértolas, B.; Hill, A. K.; García, T.; Solsona, B.; Torrente-Murciano, L. In-situ synthesis of hydrogen peroxide in tandem with selective oxidation reactions: A mini-review. *Catal. Today* **2015**, *248*, 115−127.

(16) Hou, H. L.; Zeng, X. K.; Zhang, X. W. Production of hydrogen peroxide by photocatalytic processes. *Angew. Chem., Int. Ed.* **2020**, *59*, 17356−17376.

(17) Zhou, L.; Feng, J. R.; Qiu, B. C.; Zhou, Y.; Lei, J. Y.; Xing, M. Y.; Wang, L. Z.; Zhou, Y. B.; Liu, Y. D.; Zhang, J. L. Ultrathin g-C_3N_4 nanosheet with hierarchical pores and desirable energy band for highly efficient H_2O_2 production. *Appl. Catal., B* **2020**, *267*, 118396.

(18) Lei, J. Y.; Chen, B.; Lv, W. J.; Zhou, L.; Wang, L. Z.; Liu, Y. D.; Zhang, J. L. Robust photocatalytic H_2O_2 production over inverse opal g-C3N4 with carbon vacancy under visible light. *ACS Sustainable Chem. Eng.* **2019**, *7*, 16467−16473.

(19) Wang, W. J.; An, T. C.; Li, G. Y.; Xia, D. H.; Zhao, H. J.; Yu, J. C.; Wong, P. K. Earth-abundant Ni_2P/g-C_3N_4 lamellar nanohydrids for enhanced photocatalytic hydrogen evolution and bacterial inactivation under visible light irradiation. *Appl. Catal., B* **2017**, *217*, 570−580.

(20) Wang, W. J.; Li, G. Y.; Xia, D. H.; An, T. C.; Zhao, H. J.; Wong, P. K. Photocatalytic nanomaterials for solar-driven bacterial inactivation: recent progress and challenges. *Environ. Sci.: Nano* **2017**, *4*, 782−799.

(21) Wang, W. J.; Yu, J. C.; Xia, D. H.; Wong, P. K.; Li, Y. C. Graphene and g-C_3N_4 nanosheets cowrapped elemental alpha-Sulfur as a movel metal-free heterojunction photocatalyst for bacterial inactivation under visible-light. *Environ. Sci. Technol.* **2013**, *47*, 8724−8732.

(22) Clarizia, L.; Russo, D.; Di Somma, I.; Marotta, R.; Andreozzi, R. Homogeneous photo-Fenton processes at near neutral pH: A review. *Appl. Catal., B* **2017**, *209*, 358−371.

(23) Shiraishi, Y.; Kanazawa, S.; Kofuji, Y.; Sakamoto, H.; Ichikawa, S.; Tanaka, S.; Hirai, T. Sunlight-driven hydrogen peroxide production from water and molecular oxygen by metal-free photocatalysts. *Angew. Chem., Int. Ed.* **2014**, *53*, 13454−13459.

(24) Kofuji, Y.; Isobe, Y.; Shiraishi, Y.; Sakamoto, H.; Ichikawa, S.; Tanaka, S.; Hirai, T. Hydrogen peroxide production on a carbon nitride-boron nitride-reduced graphene oxide hybrid photocatalyst under visible light. *ChemCatChem* **2018**, *10*, 2070−2077.
(25) Yang, L. P.; Dong, G. H.; Jacobs, D. L.; Wang, Y. H.; Zang, L.; Wang, C. Y. Two-channel photocatalytic production of H_2O_2 over g-C_3N_4 nanosheets modified with perylene imides. *J. Catal.* **2017**, *352*, 274−281.
(26) Hess-Erga, O.-K.; Moreno-Andres, J.; Enger, O.; Vadstein, O. Microorganisms in ballast water: Disinfection, community dynamics, and implications for management. *Sci. Total Environ.* **2019**, *657*, 704−716.
(27) Wu, D.; You, H.; Zhang, R.; Chen, C.; Lee, D.-J. Ballast waters treatment using UV/Ag-TiO_2 + O_3 advanced oxidation process with *Escherichia coli* and *Vibrio alginolyticus* as indicator microorganisms. *Chem. Eng. J.* **2011**, *174*, 714−718.
(28) Moon, G.-h.; Kim, D.-h.; Kim, H.-i.; Bokare, A. D.; Choi, W. Platinum-like behavior of reduced graphene oxide as a cocatalyst on TiO_2 for the efficient photocatalytic oxidation of arsenite. *Environ. Sci. Technol. Lett.* **2014**, *1*, 185−190.
(29) Wang, W.; Wang, H.; Li, G.; An, T.; Zhao, H.; Wong, P. K. Catalyst-free activation of persulfate by visible light for water disinfection: Efficiency and mechanisms. *Water Res.* **2019**, *157*, 106−118.
(30) Chen, X.; Yin, H.; Li, G.; Wang, W.; Wong, P. K.; Zhao, H.; An, T. Antibiotic-resistance gene transfer in antibiotic-resistance bacteria under different light irradiation: Implications from oxidative stress and gene expression. *Water Res.* **2019**, *149*, 282−291.
(31) Sun, H.; Li, G.; Nie, X.; Shi, H.; Wong, P. K.; Zhao, H.; An, T. Systematic approach to in-depth understanding of photoelectrocatalytic bacterial inactivation mechanisms by tracking the decomposed building blocks. *Environ. Sci. Technol.* **2014**, *48*, 9412−9419.
(32) Kofuji, Y.; Ohkita, S.; Shiraishi, Y.; Sakamoto, H.; Ichikawa, S.; Tanaka, S.; Hirai, T. Mellitic Triimide-Doped Carbon Nitride as Sunlight-Driven Photocatalysts for Hydrogen Peroxide Production. *ACS Sustainable Chem. Eng.* **2017**, *5*, 6478−6485.
(33) Fukuzumi, S.; Lee, Y. M.; Nam, W. Solar-driven production of hydrogen peroxide from water and dioxygen. *Chem. - Eur. J.* **2018**, *24*, 5016−5031.
(34) Kofuji, Y.; Isobe, Y.; Shiraishi, Y.; Sakamoto, H.; Tanaka, S.; Ichikawa, S.; Hirai, T. Carbon Nitride-Aromatic Diimide-Graphene Nanohybrids: Metal-Free Photocatalysts for Solar-to-Hydrogen Peroxide Energy Conversion with 0.2% Efficiency. *J. Am. Chem. Soc.* **2016**, *138*, 10019−10025.
(35) Ng, C.; Goh, S. G.; Saeidi, N.; Gerhard, W. A.; Gunsch, C. K.; Gin, K. Y. H. Occurrence of Vibrio species, beta-lactam resistant Vibrio species, and indicator bacteria in ballast and port waters of a tropical harbor. *Sci. Total Environ.* **2018**, *610*, 651−656.
(36) Wang, W. J.; Ng, T. W.; Ho, W. K.; Huang, J. H.; Liang, S. J.; An, T. C.; Li, G. Y.; Yu, J. C.; Wong, P. K. $CdIn_2S_4$ microsphere as an efficient visible-light-driven photocatalyst for bacterial inactivation: Synthesis, characterizations and photocatalytic inactivation mechanisms. *Appl. Catal., B* **2013**, *129*, 482−490.
(37) Tanaka, T.; Shimoda, M.; Shionoiri, N.; Hosokawa, M.; Taguchi, T.; Wake, H.; Matsunaga, T. Electrochemical disinfection of fish pathogens in seawater without the production of a lethal concentration of chlorine using a flow reactor. *J. Biosci. Bioeng.* **2013**, *116*, 480−484.
(38) Li, G. Y.; Nie, X.; Gao, Y. P.; An, T. C. Can environmental pharmaceuticals be photocatalytically degraded and completely mineralized in water using g-C_3N_4/TiO_2 under visible light irradiation?-Implications of persistent toxic intermediates. *Appl. Catal., B* **2016**, *180*, 726−732.
(39) Li, G. Y.; Nie, X.; Chen, J. Y.; Jiang, Q.; An, T. C.; Wong, P. K.; Zhang, H. M.; Zhao, H. J.; Yamashita, H. Enhanced visible-light-driven photocatalytic inactivation of Escherichia coli using g-C_3N_4/TiO_2 hybrid photocatalyst synthesized using a hydrothermal-calcination approach. *Water Res.* **2015**, *86*, 17−24.
(40) Brillas, E.; Sires, I.; Oturan, M. A. Electro-Fenton process and related electrochemical technologies based on fenton's reaction chemistry. *Chem. Rev.* **2009**, *109*, 6570−6631.
(41) Zhou, L.; Lei, J.; Wang, L.; Liu, Y.; Zhang, J. Highly efficient photo-Fenton degradation of methyl orange facilitated by slow light effect and hierarchical porous structure of Fe_2O_3 -SiO_2 photonic crystals. *Appl. Catal., B* **2018**, *237*, 1160−1167.
(42) Sedaghat, M.; Vahid, B.; Aber, S.; Rasoulifard, M. H.; Khataee, A.; Daneshvar, N. Electrochemical and photo-assisted electrochemical treatment of the pesticide imidacloprid in aqueous solution by the Fenton process: effect of operational parameters. *Res. Chem. Intermed.* **2016**, *42*, 855−868.
(43) Xu, T.; Zhu, R.; Zhu, G.; Zhu, J.; Liang, X.; Zhu, Y.; He, H. Mechanisms for the enhanced photo-Fenton activity of ferrihydrite modified with $BiVO_4$ at neutral pH. *Appl. Catal., B* **2017**, *212*, 50−58.
(44) Ishibashi, K.; Fujishima, A.; Watanabe, T.; Hashimoto, K. Detection of active oxidative species in TiO_2 photocatalysis using the fluorescence technique. *Electrochem. Commun.* **2000**, *2*, 207−210.
(45) Ng, T. W.; An, T. C.; Li, G. Y.; Ho, W. K.; Yip, H. Y.; Zhao, H. J.; Wong, P. K. The role and synergistic effect of the light irradiation and H_2O_2 in photocatalytic inactivation of Escherichia coli. *J. Photochem. Photobiol., B* **2015**, *149*, 164−171.
(46) Guan, H. M.; Zhu, L. H.; Zhou, H. H.; Tang, H. Q. Rapid probing of photocatalytic activity on titania-based self-cleaning materials using 7-hydroxycoumarin fluorescent probe. *Anal. Chim. Acta* **2008**, *608*, 73−78.
(47) Xiao, K. M.; Wang, T. Q.; Sun, M. Z.; Hanif, A.; Gu, Q. F.; Tian, B. B.; Jiang, Z. F.; Wang, B.; Sun, H. L.; Shang, J.; Wong, P. K. Photocatalytic bacterial inactivation by a rape Pollen-MoS_2 biohybrid catalyst: Synergetic Effects and inactivation mechanisms. *Environ. Sci. Technol.* **2020**, *54*, 537−549.
(48) Wang, W.; Zhang, L.; An, T.; Li, G.; Yip, H.-Y.; Wong, P.-K. Comparative study of visible-light-driven photocatalytic mechanisms of dye decolorization and bacterial disinfection by B-Ni-codoped TiO_2 microspheres: The role of different reactive species. *Appl. Catal., B* **2011**, *108*, 108−116.
(49) Al-Hashimi, A. M.; Mason, T. J.; Joyce, E. M. Combined effect of ultrasound and ozone on bacteria in water. *Environ. Sci. Technol.* **2015**, *49*, 11697−11702.
(50) Cheng, Y. W.; Chan, R. C. Y.; Wong, P. K. Disinfection of Legionella pneumophila by photocatalytic oxidation. *Water Res.* **2007**, *41*, 842−852.
(51) Suryo Rahmanto, A.; Pattison, D. I.; Davies, M. J. Photo-oxidation-induced inactivation of the selenium-containing protective enzymes thioredoxin reductase and glutathione peroxidase. *Free Radical Biol. Med.* **2012**, *53*, 1308−1316.
(52) Carre, G.; Hamon, E.; Ennahar, S.; Estner, M.; Lett, M.-C.; Horvatovich, P.; Gies, J.-P.; Keller, V.; Keller, N.; Andre, P. TiO_2 photocatalysis damages lipids and proteins in Escherichia coli. *Appl. Environ. Microbiol.* **2014**, *80*, 2573−2581.
(53) Li, G. Y.; Liu, X. L.; Zhang, H. M.; An, T. C.; Zhang, S. Q.; Carroll, A. R.; Zhao, H. J. In situ photoelectrocatalytic generation of bactericide for instant inactivation and rapid decomposition of Gram-negative bacteria. *J. Catal.* **2011**, *277*, 88−94.
(54) Sun, H. W.; Li, G. Y.; Nie, X.; Shi, H. X.; Wong, P. K.; Zhao, H. J.; An, T. C. Systematic approach to in-depth understanding of photoelectrocatalytic bacterial inactivation mechanisms by tracking the decomposed building blocks. *Environ. Sci. Technol.* **2014**, *48*, 9412−9419.
(55) Trubetskoj, O. A.; Richard, C.; Voyard, G.; Marchenkov, V. V.; Trubetskaya, O. E. Molecular size distribution of fluorophores in aquatic natural organic matter: Application of HPSEC with multi-wavelength absorption and fluorescence detection following LPSEC-PAGE fractionation. *Environ. Sci. Technol.* **2018**, *52*, 5287−5295.
(56) Zhao, C.; Wang, Z.; Wang, C.; Li, X.; Wang, C.-C. Photocatalytic degradation of DOM in urban stormwater runoff with TiO_2 nanoparticles under UV light irradiation: EEM-PARAFAC analysis and influence of co-existing inorganic ions. *Environ. Pollut.* **2018**, *243*, 177−188.

https://doi.org/10.1021/acsestwater.1c00048
ACS EST Water 2021, 1, 1483−1494

(57) Yamashita, Y.; Tanoue, E. Chemical characterization of protein-like fluorophores in DOM in relation to aromatic amino acids. *Mar. Chem.* **2003**, *82*, 255−271.
(58) Smith, C. B.; Anderson, J. E.; Webb, S. R. Detection of Bacillus endospores using total luminescence spectroscopy. *Spectrochim. Acta, Part A* **2004**, *60*, 2517−2521.
(59) He, D. Y.; Zhang, Z. C.; Xing, Y.; Zhou, Y. J.; Yang, H.; Liu, H. Y.; Qu, J.; Yuan, X.; Guan, J. N.; Zhang, Y. N. Black phosphorus/graphitic carbon nitride: A metal-free photocatalyst for "green" photocatalytic bacterial inactivation under visible light. *Chem. Eng. J.* **2020**, *384* (11), 123258.
(60) Spuhler, D.; Andrés Rengifo-Herrera, J.; Pulgarin, C. The effect of Fe^{2+}, Fe^{3+}, H_2O_2 and the photo-Fenton reagent at near neutral pH on the solar disinfection (SODIS) at low temperatures of water containing Escherichia coli K12. *Appl. Catal., B* **2010**, *96*, 126−141.
(61) Li, B. Q.; Ma, X. Y.; Deng, J.; Li, Q. S.; Chen, W. Z.; Li, G. X.; Chen, G. Y.; Wang, J. P. Comparison of acetaminophen degradation in UV-LED-based advance oxidation processes: Reaction kinetics, radicals contribution, degradation pathways and acute toxicity assessment. *Sci. Total Environ.* **2020**, *723*, 137993.
(62) Wu, M. N.; Wang, X. C.; Ma, X. Y. Characteristics of THMFP increase in secondary effluent and its potential toxicity. *J. Hazard. Mater.* **2013**, *261*, 325−331.

https://doi.org/10.1021/acsestwater.1c00048
ACS EST Water 2021, 1, 1483−1494